# Geothermal energy in deep aquifers

## A global assessment of the resource base for direct heat utilization

Limberger, Jon; Boxem, Thijs; Pluymaekers, Maarten; Bruhn, David; Manzella, Adele; Calcagno, Philippe; Beekman, Fred; Cloetingh, Sierd; van Wees, Jan Diederik

**DOI**
10.1016/j.rser.2017.09.084

**Publication date**
2018

**Document Version**
Final published version

**Published in**
Renewable & Sustainable Energy Reviews

**Citation (APA)**
Limberger, J., Boxem, T., Pluymaekers, M., Bruhn, D., Manzella, A., Calcagno, P., Beekman, F., Cloetingh, S., & van Wees, J. D. (2018). Geothermal energy in deep aquifers: A global assessment of the resource base for direct heat utilization. *Renewable & Sustainable Energy Reviews*, *82*, 961-975. https://doi.org/10.1016/j.rser.2017.09.084

Renewable and Sustainable Energy Reviews 82 (2018) 961–975

Contents lists available at ScienceDirect

Renewable and Sustainable Energy Reviews

journal homepage: www.elsevier.com/locate/rser

# Geothermal energy in deep aquifers: A global assessment of the resource base for direct heat utilization

Jon Limberger[a,*], Thijs Boxem[b], Maarten Pluymaekers[b], David Bruhn[c,d], Adele Manzella[e], Philippe Calcagno[f], Fred Beekman[a], Sierd Cloetingh[a], Jan-Diederik van Wees[a,b]

[a] Utrecht University, Department of Earth Sciences, PO Box 80021, 3508 TA Utrecht, The Netherlands
[b] TNO, P.O. Box 80015, NL-3508 TA Utrecht, The Netherlands
[c] Helmholtz Centre Potsdam, GFZ German Research Centre for Geosciences, Section 6.2, Telegrafenberg Building A 69, 14473 Potsdam, Germany
[d] TU-Delft, Faculty of Civil Engineering and Geosciences, PO-Box 5048, 2600 GA Delft, The Netherlands
[e] National Research Council of Italy, Institute for Geosciences and Earth Resources, Via Moruzzi 1–56124, Pisa, Italy
[f] Bureau de Recherches Géologiques et Minières (BRGM), Orléans, France

ARTICLE INFO

*Keywords:*
Geothermal energy
Global resources
Heat flow
Heat in place
Direct heat utilization

ABSTRACT

In this paper we present results of a global resource assessment for geothermal energy within deep aquifers for direct heat utilization. Greenhouse heating, spatial heating, and spatial cooling are considered in this assessment. We derive subsurface temperatures from geophysical data and apply a volumetric heat-in-place method to improve current global geothermal resource base estimates for direct heat applications. The amount of thermal energy stored within aquifers depends on the Earth's heat flow, aquifer volume, and thermal properties. We assess the thermal energy available by estimating subsurface temperatures up to a depth of three kilometer depending on aquifer thickness. The distribution of geothermal resources is displayed in a series of maps and the depth of the minimum production temperature is used as an indicator of performance and technical feasibility. Suitable aquifers underlay 16% of the Earth's land surface and store an estimated $4{\cdot}10^5$ to $5{\cdot}10^6$ EJ that could theoretically be used for direct heat applications. Even with a conservative recovery factor of 1% and an assumed lifetime of 30 years, the annual recoverable geothermal energy is in the same order as the world final energy consumption of 363.5 EJ $yr^{-1}$. Although the amount of geothermal energy stored in aquifers is vast, geothermal direct heat applications are currently underdeveloped with less than one thousandth of their technical potential used.

## 1. Introduction

### 1.1. Background

Geothermal energy is heat that is stored in the subsurface and is a renewable resource that can be sustainably exploited. Humans have had a long history of using geothermal energy for heating, cooking, and bathing [1,2]. In 1904, in the Lardarello area in Tuscany, Italy, the beginning of a new geothermal era was marked by the first successful attempt to power a light bulb with electricity converted from geothermal heat (e.g. [2,3]). Today, electricity forms an essential part of modern life, but it is often overlooked that heat production accounts for more than half of the world final energy consumption [4]. Three quarters of this heat demand is currently met by fossil fuels [4], causing a significant impact on climate and environment [5].

### 1.2. Rationale and structure of the review

The key objective of this paper is to give an overview of low-enthalpy ( < 150 °C) geothermal heat available in sedimentary aquifers suitable for direct utilization. An overview of the literature is given in Section 2, where we discuss geothermal energy in sedimentary aquifers, geothermal potential, production, installed capacity, and resource assessments. In Section 3, we present our global assessment of the geothermal resource base for direct heat. To quantify technical and theoretical potential, we apply a volumetric heat-in-place method. We explain how aquifer volume is derived and how associated subsurface temperatures are calculated using global geological and geophysical data sets. We estimate the geothermal potential for generalized direct heat and for common applications including greenhouse heating, spatial heating, and spatial cooling. We present our results in a series of maps that are made available online via a webGIS viewer: http://

* Corresponding author.
*E-mail address:* J.Limberger@uu.nl (J. Limberger).

http://dx.doi.org/10.1016/j.rser.2017.09.084
Received 28 November 2016; Received in revised form 3 August 2017; Accepted 24 September 2017
Available online 07 October 2017

thermogis.nl/worldviewer. We discuss our results in Section 3.3, before we arrive to the main conclusions in Section 4.

## 2. Literature review

### 2.1. Geothermal systems in deep aquifers

Deep ( > 100 m) geothermal aquifers are permeable layers of fluid-bearing rocks. Part of the heat that flows from the Earth's internals to its surface is stored in these aquifers and can be used directly for heating and cooling. When subsurface temperatures are sufficiently high, the heat can also be used to generate electricity. Apart from elevated temperatures in the subsurface, geothermal aquifers require high permeability to sustain flow rates that allow efficient transport of warm water from the aquifer to the surface. Sufficient permeability can occur naturally or it can be enhanced by stimulating the aquifer. Breede et al. [6], Olasolo et al. [7] and Lu [8] provide comprehensive reviews of existing enhanced geothermal systems including reservoir stimulation techniques that have been applied.

Similar to other deep subsurface activities that change temperature and pressure conditions in and around a reservoir, there is a small risk that geothermal activities cause mechanical failure of rocks and faults that could lead to seismicity [9]. To maintain public support for geothermal energy projects it is vital to prevent and minimize induced seismicity. Safe drilling, stimulation, and plant operation require sufficient understanding of subsurface structures and stress regime [10]. Gaucher et al. [11] review approaches to forecast induced seismicity, especially relevant for geothermal projects where faults are the main target for permeability or where reservoir stimulation is used to increase permeability.

Typical geothermal systems for direct heat consist of two or more wells: hot water is produced by production wells, while injection wells are used to re-inject the water after heat has been extracted. Re-injection is applied to preserve aquifer pressure allowing sustainable production and to prevent environmental contamination at the surface from geothermal fluids [12,13]. The cold water front created at the end of the re-injection well slowly migrates to the area of the production well, which eventually leads to thermal break-through. This severely reduces the efficiency of the geothermal system and marks the end of its lifetime (e.g. [14]). For doublet lifetime, it is important to consider well spacing [15] and the anisotropy of aquifer permeability [16]. The well-layout of most systems is designed to produce energy efficiently for a period of at least 30 years. Geothermal systems have been producing from the Dogger limestone aquifers in the Paris basin in France since the 1970's, which proves that lifetimes of 30 years or more are feasible [17]. Axelsson [18] lists other examples of sustained geothermal production, including a low-enthalpy system in Iceland that has been operational since the 1930's.

Lifetimes of geothermal systems can be extended up to 100 years by drilling new production and injection wells [19,20] or by optimizing production to a more sustainable rate (e.g. [21]). Compared to fossil fuel-based energy systems, geothermal energy systems are considered renewable since the time it takes to replenish 95% of the extracted heat is in the same order as the lifetime of the system [22]. Apart from technical and economical indicators, sustainability of geothermal energy can be assessed in a broader way, taking into account impact on environment and society [23]. Life cycle assessments show that geothermal energy plants have a significantly lower environmental footprint than fossil fuel-based plants [24–26] and that they are competitive with other forms of renewable energy [27].

### 2.2. Geothermal potential, production and installed capacity

In 2016, installed geothermal capacity for direct heat was 20.6 GW (equivalent electric power) [28,29], while installed geothermal capacity for electricity generation was 13.5 GW [30,31,29]. To date, the contribution of geothermal energy systems to the total energy mix has been limited: 0.15% or 0.565 EJ $yr^{-1}$ of the world final energy consumption in 2015 (363.5 EJ $yr^{-1}$) [31,28,29]. Approximately 50% (0.286 EJ $yr^{-1}$ excluding ground source heat pumps) is used for direct heat applications [28,29]. This accounts for less than 1% of the lower limit of the global geothermal resource base for direct heat, estimated by Stefansson [32] to be 32 EJ $yr^{-1}$.

By 2050, the International Energy Agency (IEA) [33] estimate geothermal production to be 5.8 EJ $yr^{-1}$ for heat (3.9% of projected world final energy for heat) and 1400 TW h $yr^{-1}$ for electricity (3.5% of projected world electricity production). In total, this production could avoid emission of almost 900 Mt $yr^{-1}$ of $CO_2$[34,33]. Goldstein et al. [35] project a 27-fold increase of current geothermal heat production to 7.8 EJ $yr^{-1}$ in 2050.

One of the main causes for the large mismatch between potential estimates and developed geothermal resources has to be sought in high up-front costs for drilling wells and associated financial risks related to geological uncertainties (e.g. [36,37]). During the exploration phase of a geothermal project, significant investments are required to de-risk prospects and to investigate their technical and economic feasibility. Drilling costs of a geothermal exploration well can easily comprise 15% of the total capital costs (CAPEX) [33,38].

Geological uncertainties and financial risks make it difficult for project developers to raise capital and to obtain insurance contracts [4]. Decentralized production of geothermal heat and the lack of uniformity among geothermal projects complicate governmental support policies to remove financial barriers (e.g. tax incentives and feed-in-tariffs for renewable energy or guarantee schemes for geothermal projects [39]) and non-financial barriers (e.g. adjusting regulation and legislation) (e.g [40,41]).

### 2.3. Geothermal resource assessments

Soaring prices of fossil fuels caused by the oil-crises of 1973 and 1979 stimulated research to quantify the potential of alternative energy sources including geothermal energy. The United States Geological Survey (USGS) developed a volumetric heat-in-place method [42,43], which has been used to estimate geothermal resources for global and regional and assessments (e.g. [32,44–46]). For this method, the area or region below the Earth's surface is divided into separate volumes. For each volume, the thermal energy in place (heat in place) is estimated based on measured or modelled subsurface temperatures.

Estimating the heat in place is straightforward, but it is more difficult to delimit the share that is technically producible. To direct this issue, it is common to apply an average value for the recovery factor to obtain the technical potential (e.g. [47]). However, little data are available on actual recovery factors, making it hard to assess whether a chosen recovery factor is realistic and appropriate for resource assessments of individual basins or entire regions [48]. More realistic recovery factors are used when data on location-specific aquifer permeability and temperature are available. For areas without any prior information or for global-scale assessments, a low recovery factor of is more appropriate [43,48]. A conservative recovery factor may lead to significant local underestimations, especially for well-explored and developed geo-ther-mal areas [43,48]. These are likely compensated by overestimation of the geothermal potential in parts of the world that have not yet been explored for geo-resources.

One of the main challenges for all resource assessments is uncertainty quantification, especially when dealing with geological data. Volumetric resource assessments are therefore often combined with probabilistic methods like the Monte-Carlo method (e.g. [36,49]). Multiple model runs yield a probability distribution of the potential, by allowing variation in parameters. It is crucial not to be overly restrictive with the ranges of allowed parameter variation and to include non-likely scenarios, since not all parameters will follow a Gaussian distribution [48,50]. Uncertainty quantification for a global geothermal

resource assessment is challenging because it requires assumptions on suitable ranges for parameters that can show a strong spatial variation and that depend on local unknown geological conditions.

## 3. Global geothermal resource base for direct heat in deep aquifers

This section is used to describe the method we use for our resource assessment and to present the results. A global overview of the resource base for direct heat applications is given and the spatial distribution of geothermal potential is presented in a series of maps. Following, we compare these results with other studies and discuss the limitations of our work.

### 3.1. Methodology

#### 3.1.1. Aquifer thickness and volume

In general, permeability of sedimentary rocks decreases with depth. This is caused by the decline in porosity, described by mechanical compaction models like Athy's law [51]. For this study, we assume a conservative fixed porosity of 15% throughout the whole aquifer. This value is representative for sedimentary formations with sandstone and shale (Fig. 1) and is based on Athy's effective stress law adapted to burial loads (c.f. [52]).

We base our aquifer thickness on a compilation of different global and regional data sets for sediment thickness. For Europe, we use the sedimentary thickness model from Tesauro et al. [53] while the model of Laske and Masters [54] (based on maps from the Exxon Production Research Company [55]) is used for the rest of the world (Fig. 5). Values from these sedimentary thickness models are directly used as maximum depth of the aquifer ($z_{max}$).

We choose to limit the maximum depth in this study to 3 km because the largest porosity reduction for siliciclastic sediments occurs within the first few kilometers (Fig. 1), making deeper geothermal production less feasible without stimulation. This depth limit is also dictated by economics because onshore drilling costs increase exponentially with depth (e.g. [56,46]).

Not all permeability in aquifers is related to primary porosity. Pore-connectivity and secondary porosity, such as fault- and fracture-related porosity can have a much stronger control on permeability. Most crystalline rocks or very tight shales and carbonates lack primary porosity, which restricts fluid flow to faults and fractures. Depending on geological conditions (e.g. [57,58]), it is possible to enhance aquifer properties with (hydraulic) stimulation [6]. In our study, we do not make a distinction between highly permeable or lowly permeable aquifers because data are scarce and only publically available for limited regions like the Netherlands [59].

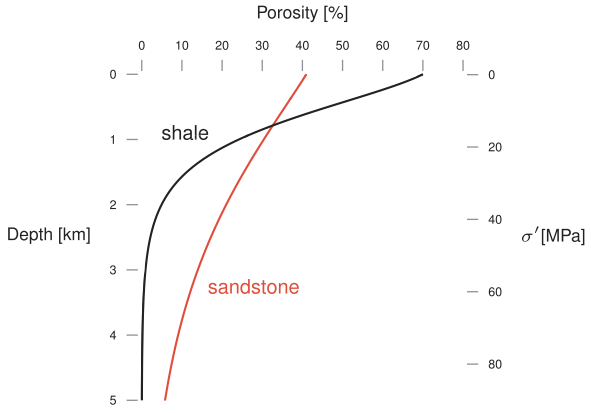


**Fig. 1.** Example of compaction curves for typical shale (black) and sandstone (red) sediments (c.f. [52]). Porosity $\phi$ (x-axis) is plotted as a function of depth and effective pressure (y-axes). (For interpretation of the references to color in this figure legend, the reader is referred to the web version of this article.)

**Table 1**
Application-specific values for minimum and maximum surface temperatures, minimum production temperatures, and re-injection temperatures.

| Application | Minimum $T_0$ | Maximum $T_0$ | Minimum $T_{prod}$ | Re-injection temperature $T_{inj}$ |
|---|---|---|---|---|
| generalized | – | – | $T_0$ + 40 °C | $T_0$ + 10 °C |
| spatial cooling | 15 °C | – | 70 °C | 35 °C |
| greenhouse heating | −15 °C | 15 °C | 45 °C | 25 °C |
| spatial heating | −15 °C | 15 °C | 70 °C | 40 °C |

#### 3.1.2. Aquifer temperature

In this section, we describe how we estimate aquifer temperatures. All geothermal systems have application-specific requirements for production temperatures and need different minimum flow rates to operate economically [60]. Temperature requirements for direct heat applications covered in our geothermal assessment are described in Section 3.1.3.

Rock thermal properties, lithosphere thickness, and heat transfer mechanisms control the heat flux through the Earth and cause most of the observed variation in subsurface temperatures. Conductive heat transfer is dominant within the Earth's lithosphere, while large-scale convective heat transfer is limited to tectonically and volcanically active areas. Regionally and locally, groundwater advection can have a strong impact on subsurface temperatures in the Earth's crust [61,62]. As listed by Bierkens [63], there are global hydrological models and data sets available for near-surface aquifers, but these do not extend to more than 100 m depth. The lack of global data on the hydrological and geothermal state of deep aquifers forces us to only consider vertical conductive heat transfer for this global assessment.

Eq. (1) shows how we calculate the maximum subsurface temperature from which we derive the geothermal gradient (See Table 2 for a list of all variables, symbols, and default values that were used in this paper):

$$\text{for } z \leq 3\text{km}: \quad T(z) = T_0 + \frac{Q_0}{k}z - \frac{A}{2k}z^2 \approx T_0 + \frac{Q_0}{k}z \tag{1}$$

For conduction-dominated regions, geothermal gradients can be estimated using both bulk thermal properties and lithosphere thickness (e.g. [64]). Geothermal gradients at the maximum depths considered for this study (up to 3 km) are largely controlled by the surface heat flow ($Q_0$) and thermal conductivity ($k$). We therefore neglect radiogenic heat production ($A$) because its contribution to the geothermal gradient is small. Fig. 2 shows that neglecting radiogenic heat generation has only minor effects on subsurface temperatures up to a depth of 3 km.

For thermal models, bulk thermal conductivity values are determined by laboratory measurements on rock samples or estimated by applying mixing rules to the thermal conductivity of the rock matrix and pore fluid (e.g. [65]). To obtain a reliable bulk thermal conductivity depth profile, mechanical compaction (Section 3.1.1) and temperature dependence need to be taken into account (c.f. [52]). For our global study, the use of these methods is severely limited without sufficient data from drill-cores or without information on in-situ geological conditions. Although bulk thermal conductivity can strongly affect geothermal gradients as shown in Fig. 2, its variability is generally less than surface heat flow and radiogenic heat generation.

For our global subsurface temperature model, we assume a fixed bulk thermal conductivity of 2 $Wm^{-1}K^{-1}$ as a base case for all aquifers and make use of publically available surface heat flow data (Fig. 6). As a starting point, we use the surface heat flow model of Artemieva [66]. It is an improved interpolation of the original data set from Pollack et al. [67] and covers most of the continents at a resolution of 5°×5°. For full map coverage, we use the global heat flow model from Davies [68] to fill the gaps. Models with higher resolution are used for Europe

**Table 2**
Input and output variables with associated symbols, units and default values.

| Output variable | Input variable | Symbol | Unit | Value |
|---|---|---|---|---|
| subsurface temperature | | $T$ | °C | |
| | surface heat flow | $Q_0$ | m $Wm^{-2}$ | |
| | surface temperature | $T_0$ | °C | |
| | bulk thermal conductivity | $k$ | $Wm^{-}$ $K^{-1}$ | 1.75; 2; 2.25 |
| | depth; min.; max. | $z$; $z_{min}$; $z_{max}$ | km | |
| heat in place | | $H$ | PJ $km^{-2}$ | |
| | aquifer thickness | $h$ | km | |
| | production temperature | $T_{prod}$ | °C | |
| | re-injection temperature | $T_{inj}$ | °C | |
| | aquifer bulk heat capacity | $\gamma$ | MJ | 2.8 |
| | porosity | $\phi$ | – | 15% |
| | heat capacity water | $C_w$ | J $kg_{-1}$ $K_{-1}$ | 1000 |
| | heat capacity aquifer rock | $C_r$ | J $kg_{-1}$ $K_{-1}$ | 3772 |
| | density water | $\rho_w$ | kg $m_{-3}$ | 1042 |
| | density aquifer rock | $\rho_r$ | $_{-3}$ | 2600 |
| theoretical potential | | $P_{theory}$ | PJ $km^{-2}$ $yr^{-1}$ | |
| | economic lifetime | $t$ | yr | 30 |
| technical potential | | $P_{technical}$ | TJ $km^{-2}$ $yr^{-1}$ | |
| | ultimate recovery factor | $UR$ | – | 1% |

[57] and the USA [69]. We assume higher heat flow values for volcanic regions based on GPS locations from the Global Volcanism Program [70] database. We adopt a strongly elevated heat flow of 140 mW $m^{-2}$ for areas with active volcanoes and a moderately elevated heat flow of 80 mW $m^{-2}$ for regions that experienced Holocene volcanic activity [71].

Combining surface heat flow data with surface temperature data (Fig. 3) allows us to extrapolate subsurface temperatures to the required depths. For the surface temperature, we use annual continental mean surface temperatures recorded between 1950 and 2000 from the WorldClim Global Climate Database from Hijmans et al. [72]. We combine this data with the model of Kalnay et al. [73] for surface temperatures of Antarctica and with the model of Boyer et al. [74] for ocean surface temperatures. As reference level, we use the ETOPO1 elevation and bathymetry model (Fig. 4) from Amante and Eakins [75].

### 3.1.3. Resource estimation

For our global geothermal resource assessment of direct heat, the total resource base is estimated, including both identified and undiscovered resources. We define the geothermal resource base as the aquifer volume with temperatures sufficiently high to meet the requirements for direct heat applications.

There are numerous non-electrical uses of geothermal energy [76–78]. For this study we use temperature requirements for generalized utilization of direct heat and for three common applications: greenhouse heating, spatial heating, and spatial cooling. We do not take into account the potential of heat that can be produced by ground source heat pumps or by cascade utilization of higher enthalpy geothermal systems [79].

Each application requires a set of temperature conditions at the surface (minimum and maximum) and in the subsurface (minimum production and re-injection temperature) [60]. In Table 1, the surface and subsurface temperature requirements are listed. The range of surface temperatures ($T_0$) is restricted to −15 °C and 15 °C for greenhouse and spatial heating, while for spatial cooling only a minimum surface temperature of 15 °C is required. For generalized direct utilization, minimum production temperatures ($T_{prod}$) are obtained by adding 40 °C to the surface temperature. Minimum re-injection temperatures ($T_{inj}$) are found by adding 10 °C to the surface temperature.

The estimated temperatures from our global thermal model are used to find the minimum depth $z_{min}$ at which the required production temperatures for the earlier described applications are reached. The effective aquifer thickness $h$ that can be theoretically used, is obtained by taking the difference between the depth of the minimum production temperature and the maximum depth $z_{max}$ (limited to a maximum of 3 km). The effective aquifer thickness is multiplied by the horizontal surface area of the grid cell, which yields the total effective aquifer volume. For our assessment we only consider areas with an aquifer thickness of more than 100 m.

Eq. (2) shows how the effective total aquifer volume can be translated into the theoretical capacity (heat in place $H$) with the use of a bulk heat capacity parameter $\gamma$ (Eq. (3)):

$$H = h \cdot (T_{prod} - T_{inj}) \cdot \gamma \quad (2)$$

$$\gamma = \phi \cdot c_w \cdot \rho_w + (1 - \phi) \cdot c_r \cdot \rho_r \quad (3)$$

The bulk heat capacity is defined by the density ($\rho_r$ and $\rho_w$) and heat capacity of aquifer rocks and fluids ($C_r$ and $C_w$) and the ratio between rocks and fluids, determined by aquifer porosity ($\phi$). All geothermal gradients estimated in this study are linear, enabling the use of mean production temperatures for each vertical column of effective volumes.

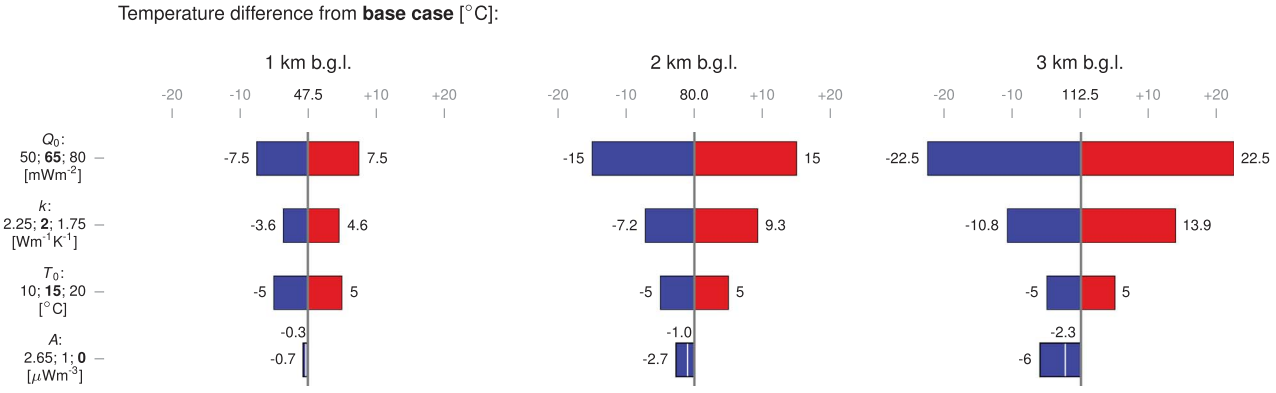


**Fig. 2.** Tornado plots showing the sensitivity of subsurface temperatures at three depth levels (1–3 km) to changes in surface heat flow ($Q_0$), thermal conductivity ($k$), surface temperature ($T_0$), and radiogenic heat production ($A$). For each parameter, three values are indicated that are used for the calculation. The values in bold are used to calculate default temperatures at each depth level. The other values are used to calculate temperature differences in respect to the default case.

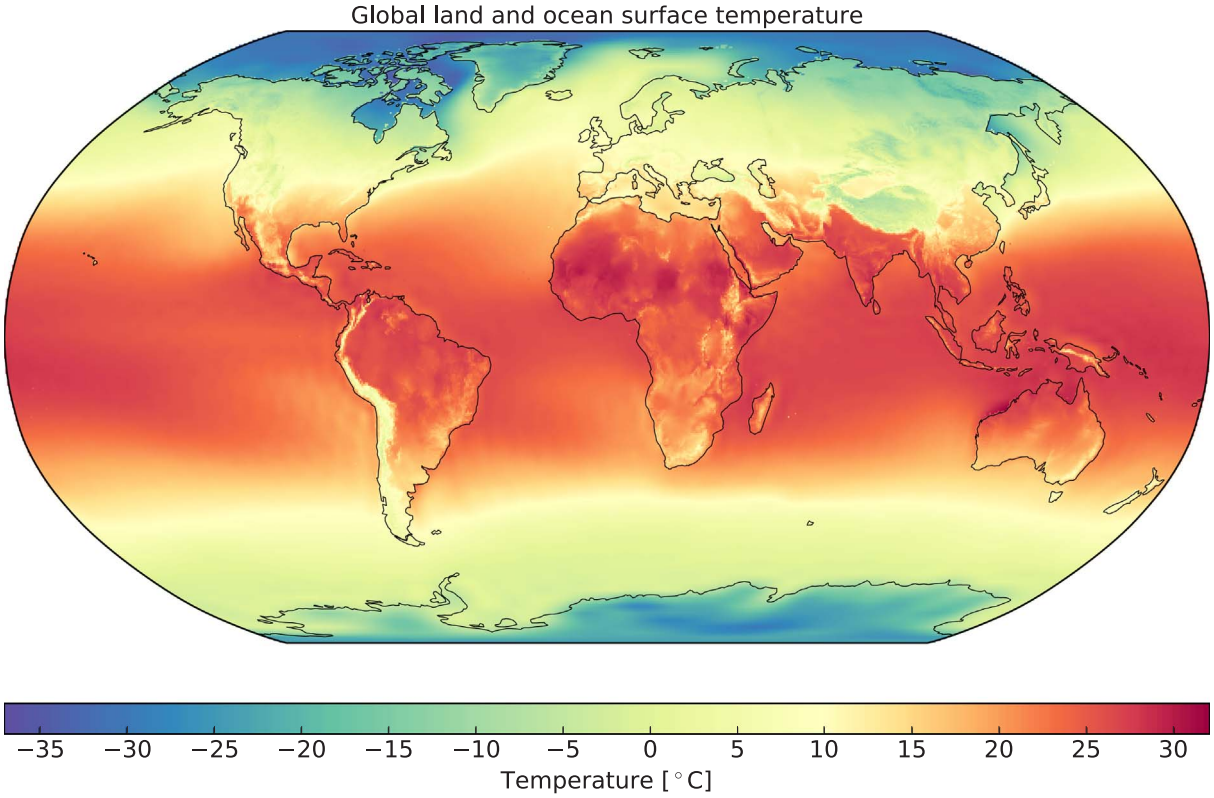


**Fig. 3.** Mean global land surface temperatures and ocean surface temperatures. Compilation based on Hijmans et al. [72], Kalnay et al. [73] (Antarctica), and Boyer et al. [74] (oceans).

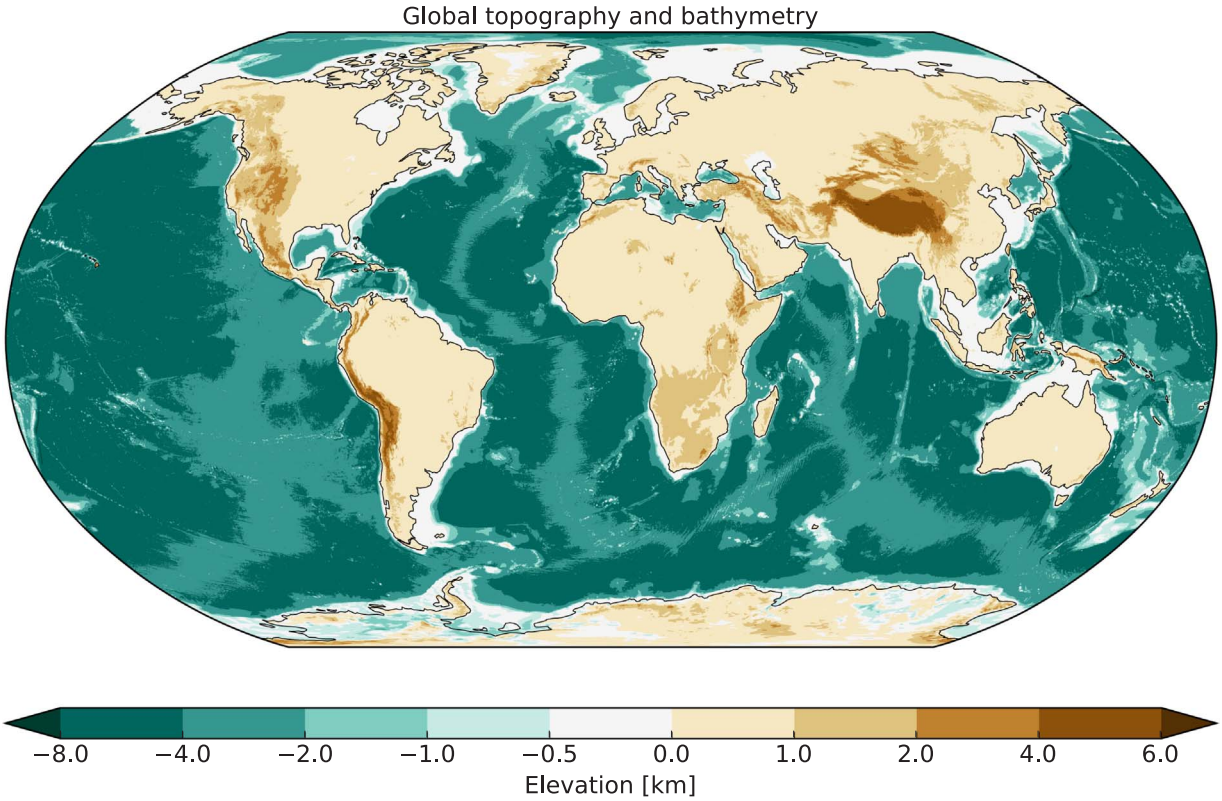


**Fig. 4.** Topography and bathymetry from ETOPO1 [75].

The heat in place that can be realistically exploited is limited by technical and economical conditions. These include surface and subsurface limitations, such as plant facilities and drilling technologies. Rybach [80] also defines two potentials that we did no consider in this study: the sustainable and developable potential. The sustainable potential is a fraction of the economical potential that can be utilized by applying sustainable production levels. The developable potential describes the fraction of the economic potential that can be developed under realistic

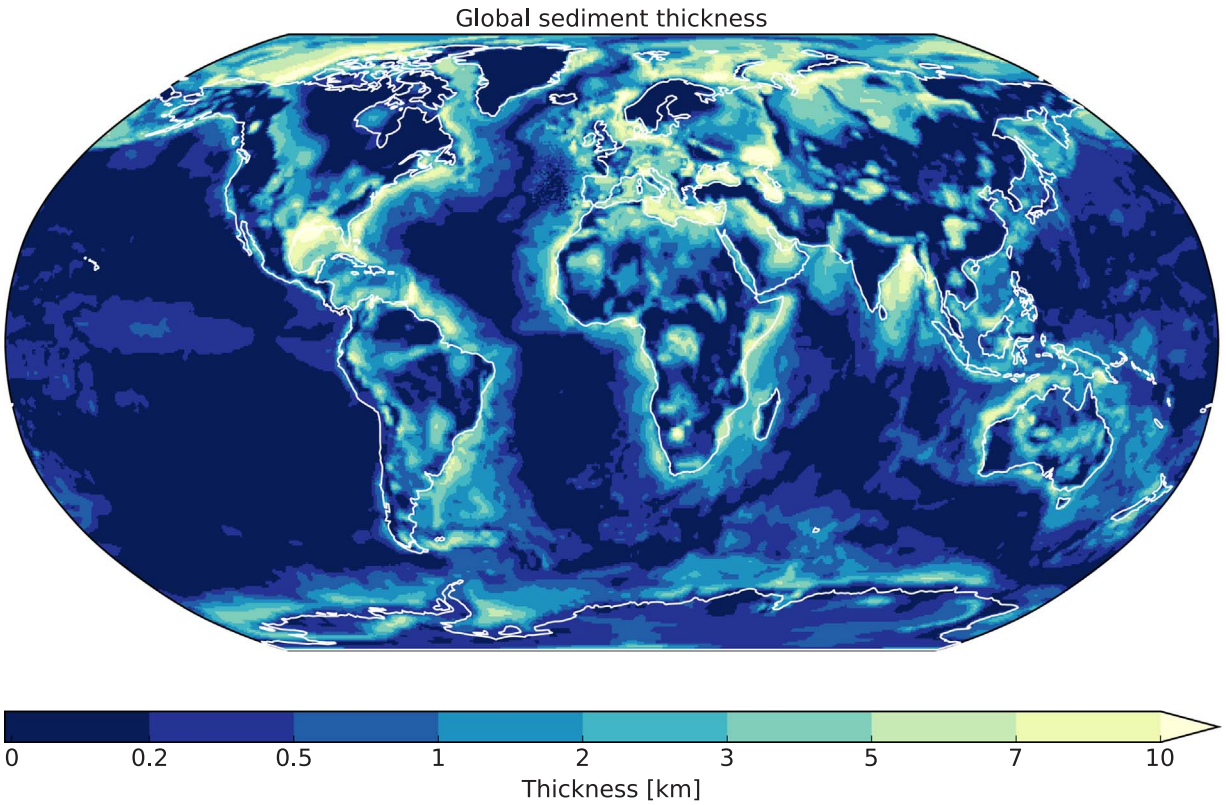


**Fig. 5.** Sediment thickness from Exxon Production Research Company [55] and Tesauro et al. [53] (Europe).

environmental, regulatory, and political limitations.

Following the outcomes of earlier large-scale assessments (e.g. [43,46]) and recommendations from the review paper of Grant [48], the technical potential is calculated as a fraction of the heat in place using a recovery factor *UR* of 1%. We further assume a system lifetime *t* of 30 years, yielding a technical potential that is 1/3000th of the heat in

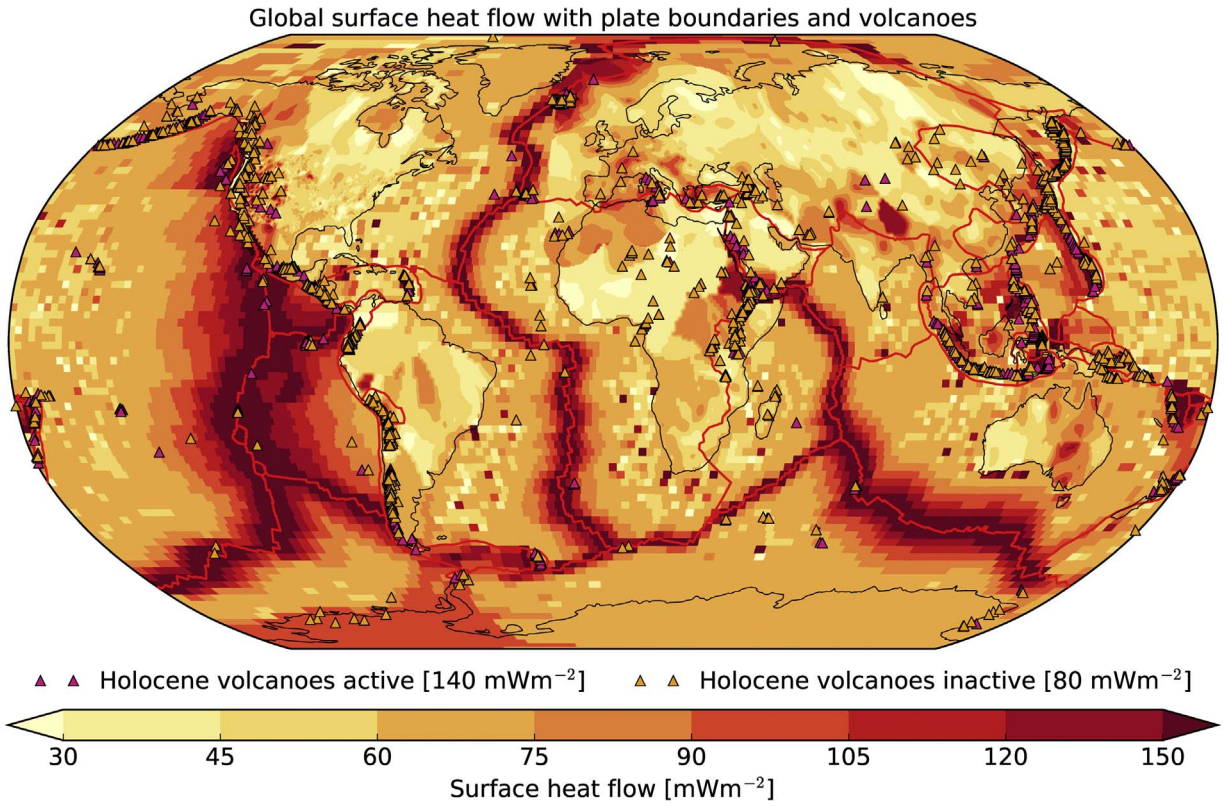


**Fig. 6.** Global surface heat flow compilation with plate boundaries and volcanoes. See Section 2.2 for details.

place (4) and (5).

$$P_{theory} = \frac{H}{t} \quad (4)$$

$$P_{technical} = P_{theory} \cdot UR \quad (5)$$

Heat production sites are preferably located in or nearby areas where the heat is to be consumed. To better assess economic feasibility (e.g. [46,49]), the technical potential can be matched to the local heat demand [81] to obtain a matched potential. However, this requires global data on the spatial distribution of heat demand (e.g. [82–84]) that is not yet available.

### 3.2. Results

Below we present the results of our geothermal potential assessment for generalized direct heat and for common applications including greenhouse heating, spatial heating, and spatial cooling.

#### 3.2.1. Global heat flow and aquifer temperature

We present the results of the temperature model with two maps. The first map (Fig. 7), showing the mean geothermal gradient within global aquifer systems, only reflects variation of the surface heat flow. The mean global heat flow for all continents and oceans from our heat flow compilation (Fig. 6) yields a value of 83 mW $m^{-2}$ with a standard deviation of 60 mW $m^{-2}$. Within aquifers, the mean heat flow is 64 mW $m^{-2}$ with a standard deviation of 25 mW $m^{-2}$. This results in a mean global aquifer geothermal gradient of 32 °C $km^{-1}$ with a standard deviation of 14 °C $km^{-1}$. High geothermal gradients are found in zones with high heat flow, most notably near active plate boundaries or other regions that have been tectonically and volcanically active.

The second map (Fig. 8) shows the maximum temperature within these aquifers, which depends both on the geothermal gradient and aquifer thickness. When aquifers are sufficiently thick, normal geothermal gradients (~30 °C $km^{-1}$) lead to relatively high temperatures. The Southern Permian Basin in Europe is an example of such a case. Thin aquifers with elevated geothermal gradients give a similar result, as can be seen in the thin aquifers surrounding the Baja California. The highest maximum temperatures are found in thick aquifers in regions with elevated geothermal gradients ( > 40 °C $km^{-1}$) such as the Pannonian Basin in Europe, the North African Basins, the foreland basins of the Himalaya, the East Java Basin, and basins in central and eastern Australia.

#### 3.2.2. Global distribution of effective aquifer volume

In Table 3 we present the total effective aquifer volume for each direct heat application, based on the total surface area of suitable aquifers and their effective thickness. Total effective aquifer volume ranges between $4.0 \cdot 10^6$ $km^3$ for spatial heating to $22.8 \cdot 10^6$ $km^3$ for generalized direct heat applications. The large variation in volume is explained by the spatial variation in aquifer thickness (Fig. 5) and geothermal gradients (Fig. 7), combined with application-specific temperature requirements (Table 1). An estimated $22.8 \cdot 10^6$ $km^3$ of total aquifer volume is available for generalized direct heat utilization. This volume covers 35% of the continental surface underlain by aquifers or 16% of the total continental surface area.

The highest effective aquifer volume ($18.2 \cdot 10^6$ $km^3$) is available for spatial cooling because a larger portion of the total aquifer volume is found at mid to low latitudes. An estimated 26% of the continental surface area underlain by aquifers and 12% of the total continental surface area are suitable for spatial cooling.

Spatial heating requires low surface temperatures in combination with high production temperatures. Low surface temperature are restricted to the high to middle latitudes, which limits usable aquifer volume compared to the other applications. For spatial heating, 7% of the continental surface underlain by aquifers or 3% of the total continental surface area is available. Greenhouse heating requires the same low surface temperatures as spatial heating, but does not need high production temperatures. The effective aquifer volume of $9.9 \cdot 10^6$ $km^3$ is

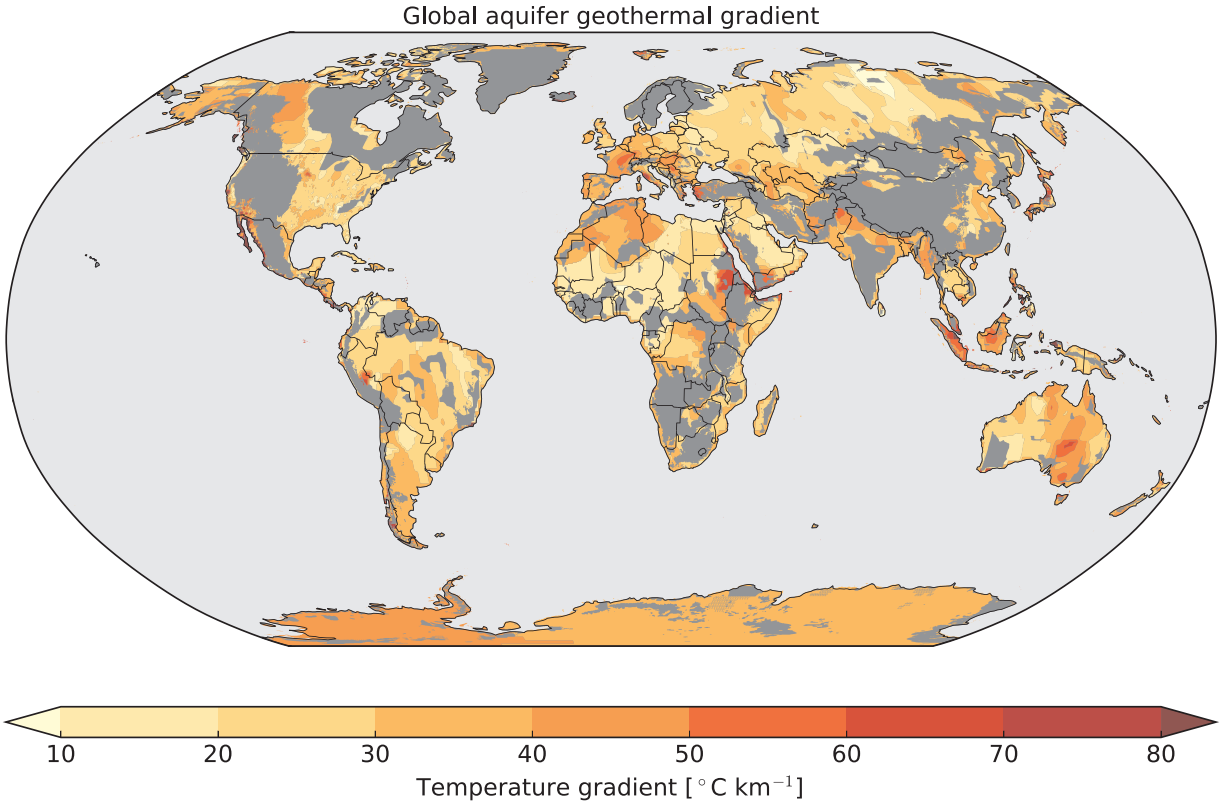


**Fig. 7.** Computed geothermal gradients in aquifers. Grey areas on the land surface indicate a sediment thickness less than 100 m and are not considered in this study.

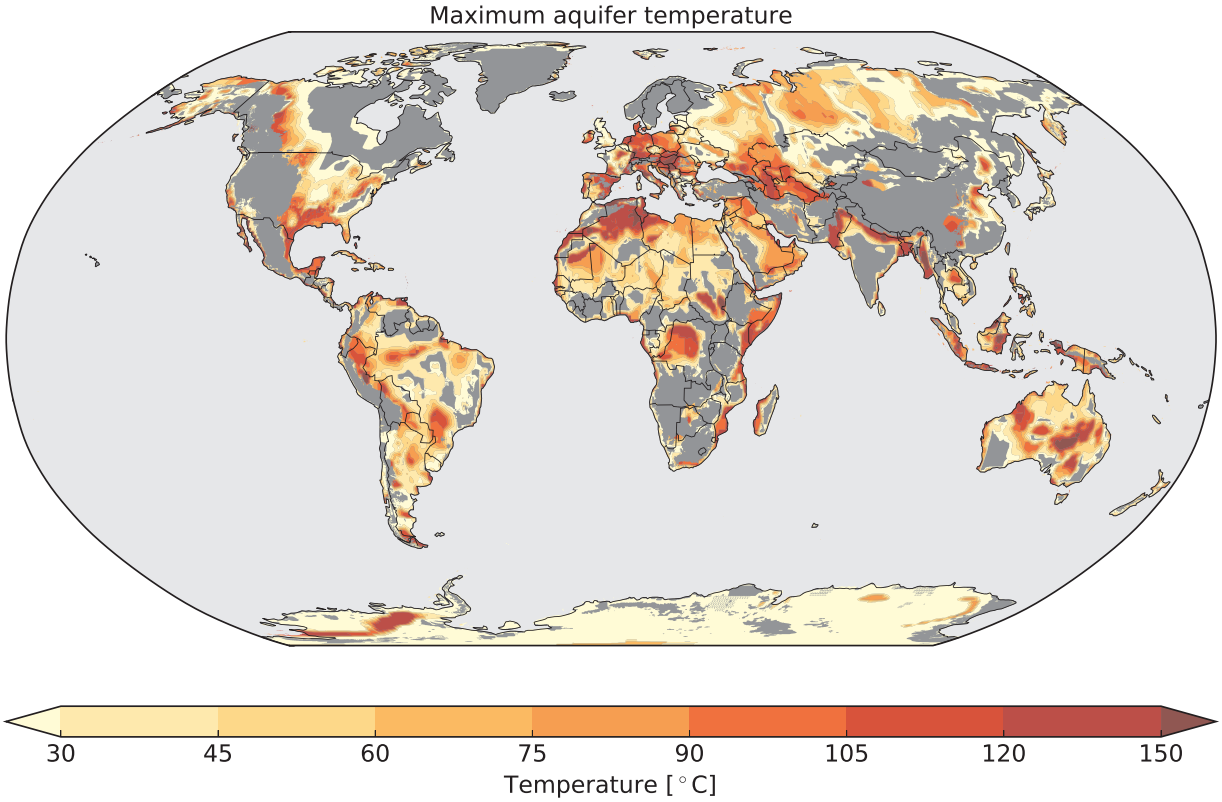


**Fig. 8.** Computed maximum aquifer temperature $T_{max}$. Temperatures depend on the geothermal gradient and maximum aquifer thickness. Temperatures are only computed to a maximum depth of 3 km. Grey areas on the land surface indicate a sediment thickness less than 100 m and are not considered in this study.

**Table 3**
Overview of results including total available aquifer volume, surface area, coverage, heat in place, and technical potential. Total aquifer volume and surface area are based on the spatial distribution of effective aquifer thickness which depends on geothermal gradient, application-specific temperature requirements, and gross aquifer thickness. Coverage is expressed as a percentage of the total aquifer surface area of $70.5 \cdot 10^6$ km$^2$ and as a percentage of the total continental surface area of $149 \cdot 10^6$ km$^2$. The heat in place and technical potential are calculated for each application and for three different thermal conductivities to show the impact of geological uncertainty on the resource assessment results.

| Application | Total aquifer: | | | Total aquifer: | | | | | |
|---|---|---|---|---|---|---|---|---|---|
| | volume [$10^6$ km$^3$] | area [$10^6$ km$^2$] | coverage [%] | heat in place [$10^6$ EJ*] | | | technical potential [EJ* yr$^{-1}$] | | |
| | | | | $k = 1.75$ | $k = 2$ | $k = 2.25$ | $k = 1.75$ | $k = 2$ | $k$ 2.25 |
| generalized | 22.8 | 24.5 | 35 & 16 | 5.38 | 4.03 | 3.02 | 1793 | 1345 | 1005 |
| spatial cooling | 18.2 | 18.2 | 26 & 12 | 3.95 | 3.03 | 2.33 | 1316 | 1011 | 778 |
| greenhouse heating | 9.9 | 8.9 | 13 & 6 | 1.60 | 1.24 | 0.97 | 533 | 413 | 324 |
| spatial heating | 4.0 | 5.2 | 7 & 3 | 0.84 | 0.56 | 0.37 | 278 | 187 | 125 |

* 1 EJ = $10^6$ TJ = $10^{18}$ J

larger than for spatial heating, but is more restricted to higher latitudes. Regions suitable for greenhouse heating cover 13% of the continental surface underlain by aquifers or 6% of the total continental surface area.

### 3.2.3. Geothermal resource base

In the next series of maps (Figs. 9–16), we present the spatial distribution of the geothermal resource base in deep aquifers for direct heat. For each of the different applications, we present the technical potential and a qualitative performance indicator. The performance indicator maps give an indication of economic feasibility for each application by showing their attractiveness based on the minimum required production depth ($z_{min}$). Minimum production depths up to 600 m are considered excellent, up to 1200 m very good, up to 1800 m good, up to 2400 m moderate, and poor for more than 2400 m.

To show the impact of geological uncertainty on this resource assessment, we vary thermal conductivity with ± 0.25 Wm$^{-1}$ K$^{-1}$. This has a strong effect on the geothermal gradient and determines the final estimates for the geothermal potential (see Table 3). A slight increase (+12.5%) of the thermal conductivity reduces the total aquifer technical potential with 25–33% depending on the application. Decreasing (−12.5%) thermal conductivity results in a 29–49% increase in technical potential. In the following paragraphs, we discuss the results of the case with a default thermal conductivity of 2 Wm$^{-1}$ K$^{-1}$.

The global technical potential for generalized direct heat (Fig. 9) is 52 TJ yr$^{-1}$ km$^{-2}$. Since we did not use any surface temperature constraints for this case, the spatial distribution only reflects maximum aquifer temperatures (Fig. 8). Potential economic feasibility based on minimum production depths is shown in Fig. 10. We estimate a total

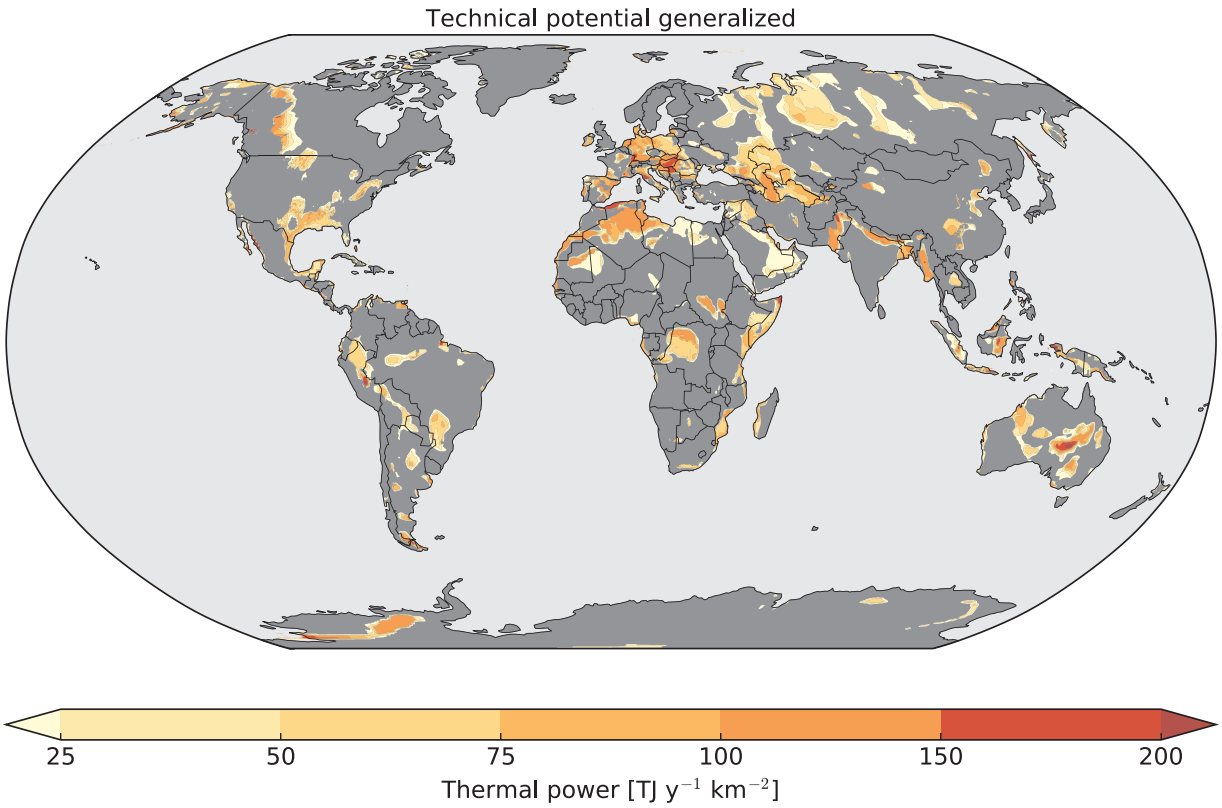


**Fig. 9.** Technical potential for all direct heat applications combined. For this and the following figures, the grey color on the land surface indicates regions with an effective aquifer thickness less than 100 m or regions where application-specific (sub) surface temeprature requirements are not met.

heat in place of $4.03 \cdot 10^6$ EJ and technical potential of 1345 EJ yr$^{-1}$ (Table 3).

Fig. 11 shows the technical potential of the spatial cooling case with a global technical potential of 55 TJ yr$^{-1}$ km$^{-2}$. Spatial cooling requires surface temperatures above 15 °C, restricting the technical potential to lower latitudes close to the equator (Figs. 3, 11). Potential

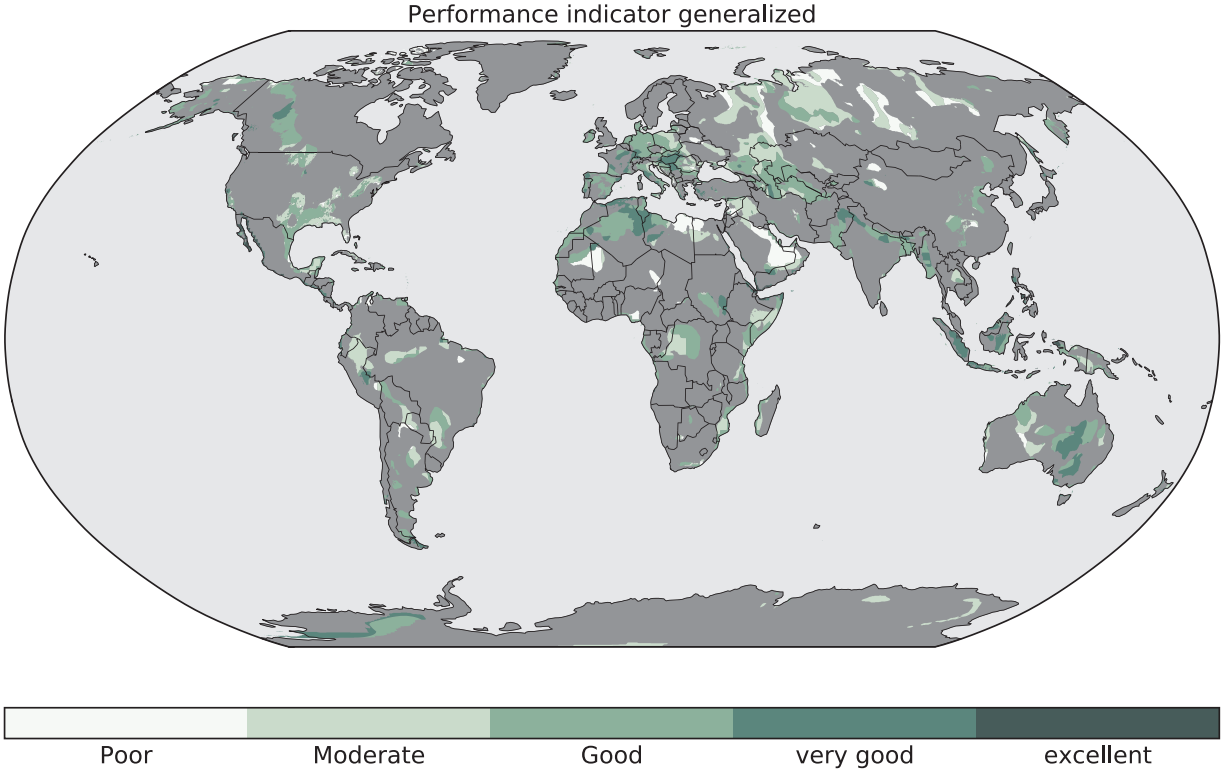


**Fig. 10.** Performance indicator for all direct heat applications combined. This qualitative indicator is shown for regions that have a technical potential and is based on the minimum production depth required for generalized direct heat use.

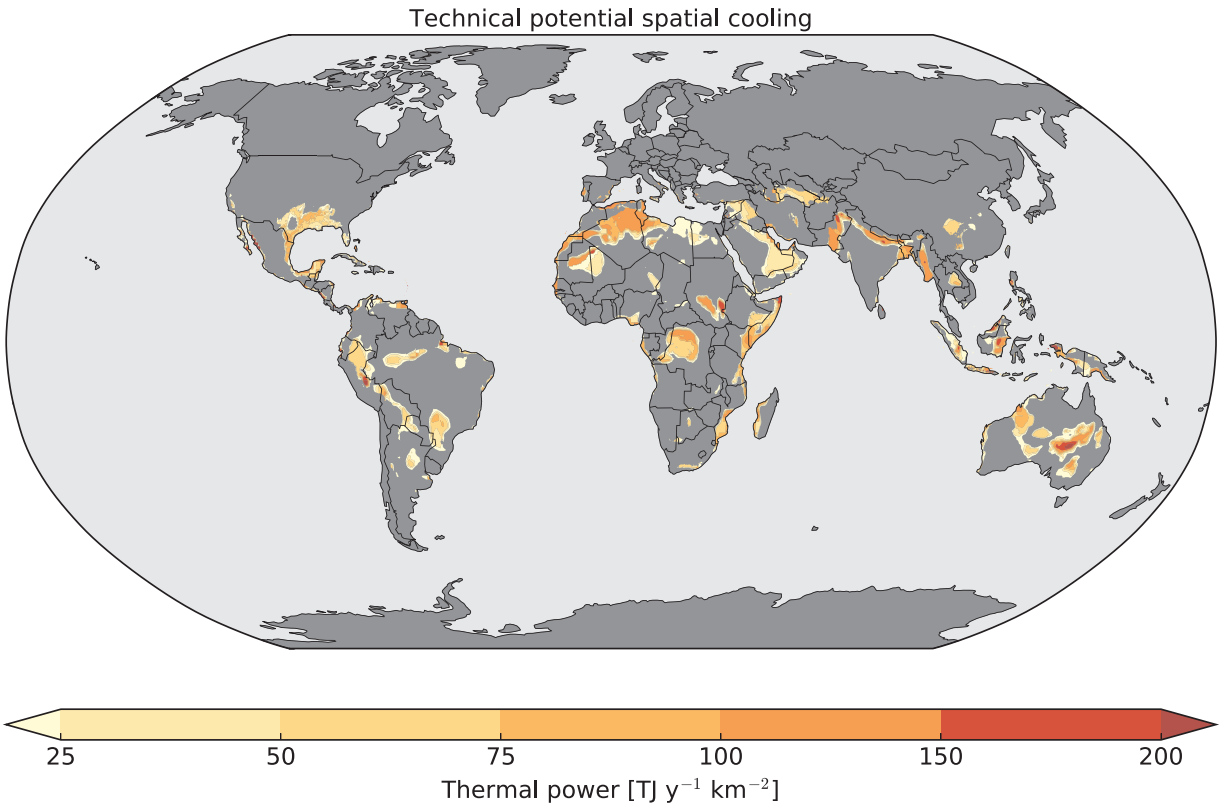


**Fig. 11.** Technical potential for spatial cooling.

economic feasibility based on minimum production depths is shown in Fig. 12. We estimate a total heat in place of 3.03 $10^6$ EJ and a technical potential of 1011 EJ yr$^{-1}$ (Table 3).

Greenhouse heating and spatial heating have an estimated global technical potential of 42 TJ yr$^{-1}$ km$^{-2}$ and 34 TJ yr$^{-1}$ km$^{-2}$. The spatial distribution (Figs. 13 and 15) is controlled by their temperature

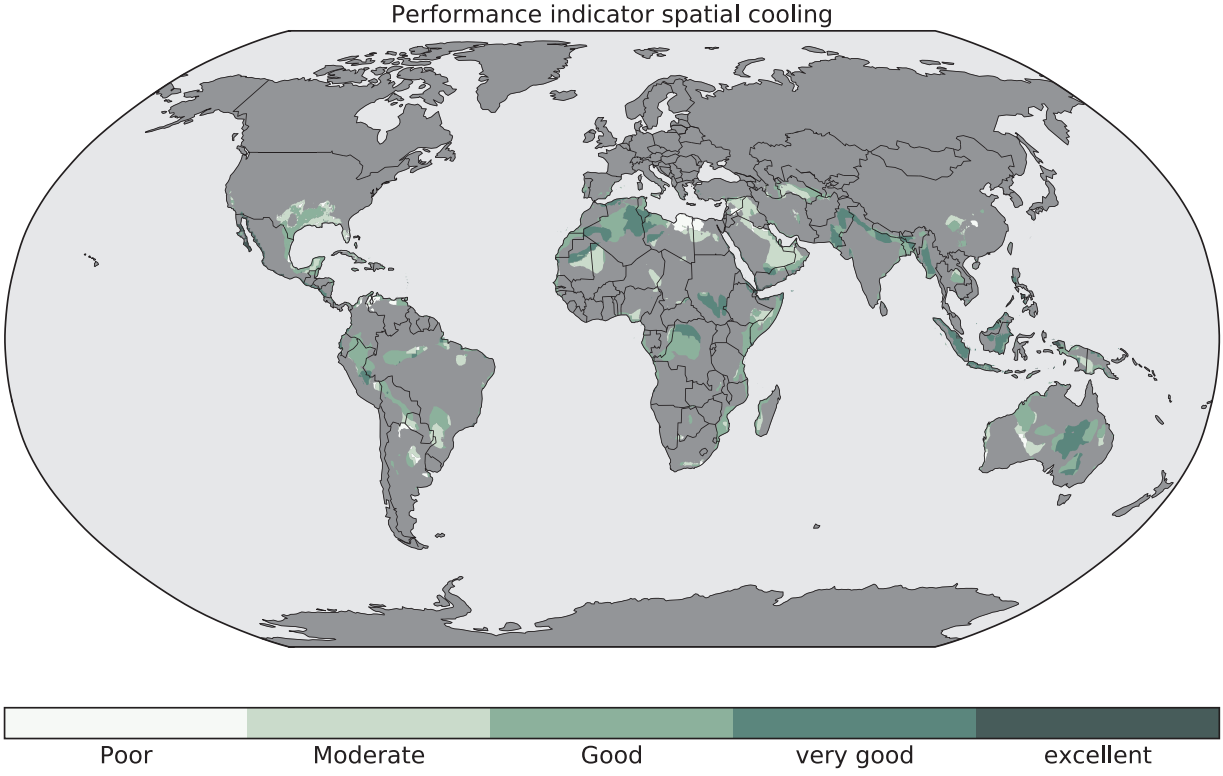


**Fig. 12.** Performance indicator for spatial cooling. This qualitative indicator is shown for regions that have a technical potential and is based on the minimum production depth required for spatial cooling.

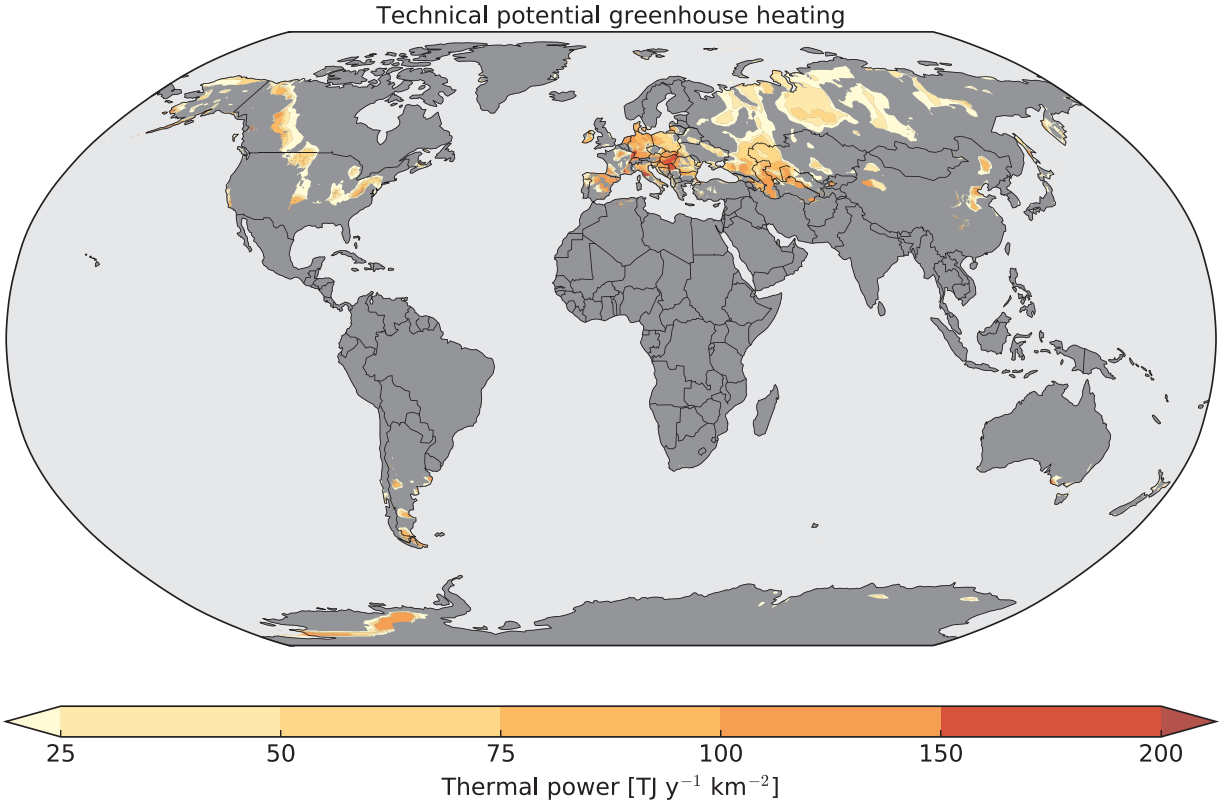


**Fig. 13.** Technical potential for greenhouse heating.

requirements and mainly follows the surface temperature variation. Both greenhouse heating and spatial heating require surface temperatures below 15 °C, more common at mid to high latitudes (Fig. 3). For greenhouse heating, we obtain a total heat in place of $1.24 \cdot 10^6$ EJ and a technical potential of 413 EJ yr$^{-1}$. For spatial heating, we estimate a total heat in place of $0.56 \cdot 10^6$ EJ and a technical potential of

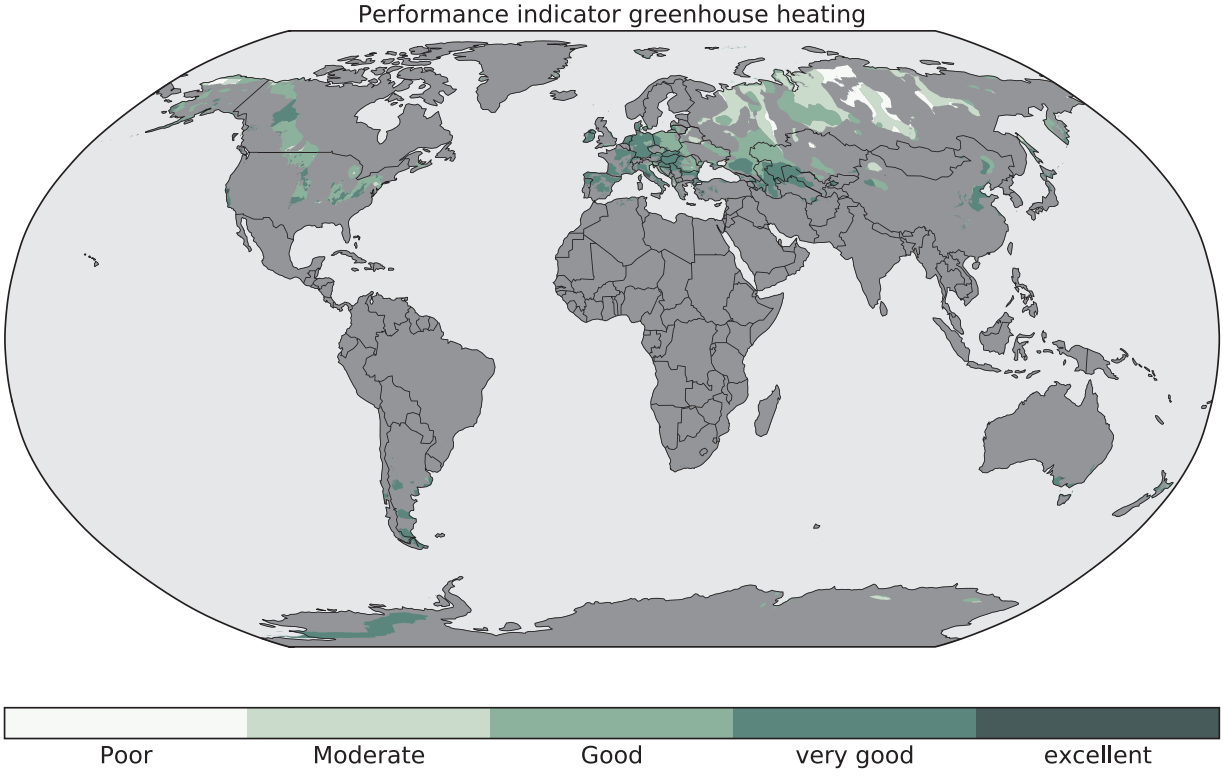


**Fig. 14.** Performance indicator for greenhouse heating. This qualitative indicator is shown for regions that have a technical potential and is based on the minimum production depth required for greenhouse heating.

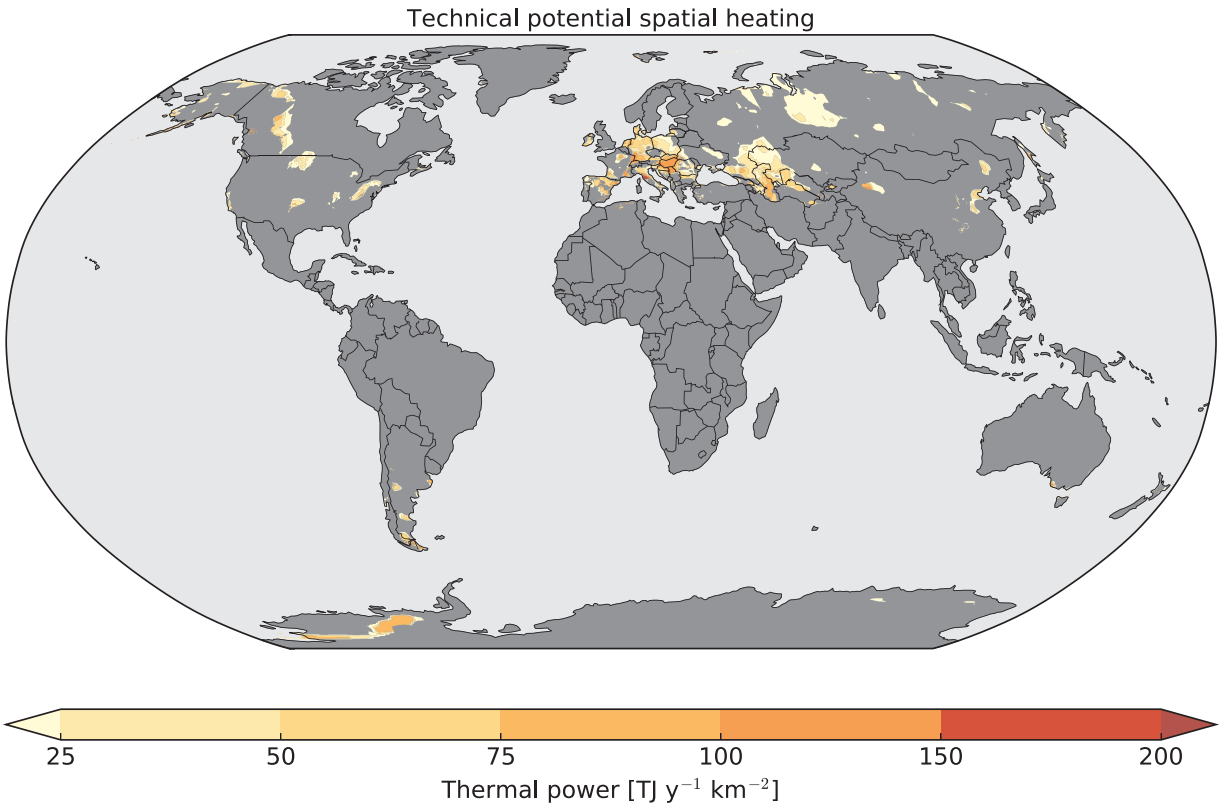


**Fig. 15.** Technical potential for spatial heating.

187 EJ yr$^{-1}$. The higher temperatures required for spatial heating (Table 1) result in a lower technical potential for spatial heating compared to greenhouse heating. This is also reflected in the potential economic feasibility maps that are based on minimum production depths (Figs. 14 and 16). In general, spatial heating requires larger depths to reach the required production temperatures.

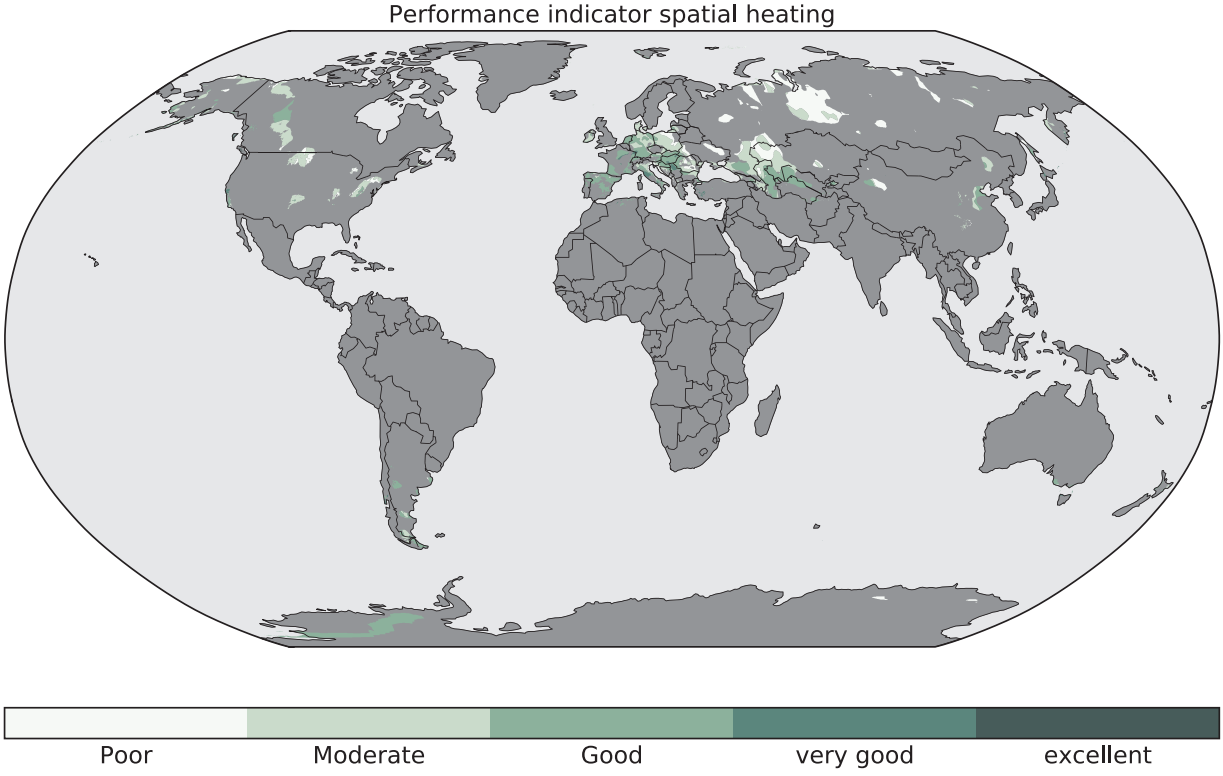


**Fig. 16.** Performance indicator for spatial heating. This qualitative indicator is shown for regions that have a technical potential and is based on the minimum production depth required for spatial heating.

### 3.3. Discussion

Quantifying uncertainty for a global geothermal resource assessment is challenging because input parameters depend on poorly constrained geological conditions. This inhibits the use of probabilistic methods for this global geothermal resource assessment. Instead, we choose to vary the thermal conductivity to show the effect of geological uncertainty on resource base estimates.

The recovery factor of 1% that we apply could be too conservative for many well-studied basins in Europe and the USA. At the same time, we do not take into account terrain accessibility and population density. For example, it is technically possible to develop geothermal systems in deserts or arctic areas. However, without sufficient inhabitants a geothermal project is economically unfeasible because there is insufficient demand for heat. Limberger et al. [46] conducted a European resource assessment for electricity from enhanced geothermal systems. They showed that a combination of well-cost models with economic assumptions similar to recent market conditions leads to a further reduction of the resource base, yielding recovery factors of 0.1–0.2%. However, large part of these high temperature resources are also located deeper, lowering recovery factors significantly due to an exponential increase of drilling costs with depths over 4 km.

Our calculated mean global heat flow is in line with other studies [67,85,68]. Total heat flow through aquifers is estimated at 134 EJ $yr^{-1}$, which is in the same order of magnitude as the technical potential estimates given in Table 3. This heat flow is sufficient to replenish the lost heat on a anthropogenic time-scale, even for the unlikely scenario where the total technical potential for the generalized case were to be utilized.

Earlier estimates on global potential for continental geothermal resources were conducted by EPRI [86]. By extrapolating a fixed geothermal gradient of 25 °C km-1 up to a depth of 3 km, assuming 15 °C at the surface, they obtained a potential of $1.4{\cdot}10^{4}$ EJ $yr^{-1}$. This is approximately 10 times our estimate of the potential of generalized direct heat applications (Table 3). This is to be expected since we only consider aquifers up to three km depth and apply a higher threshold for required production temperatures (Table 1). For our generalized case, this threshold temperature considerably limits the total available volume, down to 5% of the volume used by EPRI [86]. At the same time, our mean geothermal gradient of 32 °C $km^{-1}$ is higher than their fixed gradient of 25 °C $km^{-1}$ and our estimates are in the same range as the upper limit of 1400 EJ $yr^{-1}$ given by the global assessment of Stefansson [32].

One of the main limitations of our study is the use of a fixed thermal conductivity for all aquifers. Differences in lithology, but also effects of burial and erosion have a large impact on the thermal conductivity of aquifers (e.g. [52]). For all sedimentary rocks, we assume a fixed porosity and water as the only pore fluid. However, tight siliciclastic rocks, such as shales, typically lack large amounts of fluids. Furthermore, not all sedimentary formations are water-bearing. Some formations may contain mixtures of hydrocarbons, carbon-dioxode and water, or totally lack any fluids. As shown in Fig. 2, a small difference in thermal conductivity can drastically change the geothermal gradient.

Aquifer thickness is another source of uncertainty because we rely on the global sediment thickness model from Laske and Masters [54], largely derived from the tectonic map of the world compiled by the petroleum industry [55]. It is difficult to make a distinction between sediments and highly metamorphosed sediments based on density or velocity alone and without any constraints from wells or geophysical data. This can be a problem in old cratons and leads to over- and underestimates in aquifer volume and technical potential in areas such as the East European Craton and large parts of Australia and Africa.

Surface heat flow measurements can also have a large uncertainty. Heat flows are determined via a series of temperature measurements through a given interval. Thermal conductivity values are used to calculate the surface heat flow. In the best case, several thermal conductivity measurements are used for this calculation. Instead, it is common to only use single estimated value. It is also important to apply the appropriate corrections depending on where and how deep the measurements have been conducted. Powell et al. [87] and Beardsmore and Cull [88] review heat flow measurement methods and give a comprehensive list of corrections that should be applied including corrections for terrain and paleoclimate, transient geological processes such as sedimentation and erosion, and groundwater flow. As recently showed in a study by Kooi [62], effects of deep groundwater flow are still poorly quantified and net-cooling effects could lead to a significant underestimation of the surface heat flow.

Our heat flow compilation largely consists of global data sets that are partly based on old measurements. Some of those measurements could be of questionable quality (e.g. [67]). A large number of measurements lack an indication of data quality and information on the applied corrections. Another problem is the inhomogeneous distribution of heat flow measurements because measurements are typically conducted within regions that (possibly) contain geo-resources. Since hydrocarbon formation is generally restricted to sedimentary basins, there is a strong correlation between sedimentary basins (aquifers) and hydrocarbon exploration and exploitation. This makes data availability less of a problem for our aquifer assessment, but large uncertainties remain in underexplored regions such as Antarctica and Greenland.

A last, but vital requirement for geothermal development is heat demand. Since it is economically unfeasible to transfer heat over large distances, development of geothermal systems is restricted to urbanized and industrialized areas. The global economical and matched potential could therefore be significantly lower than our technical potential.

## 4. Conclusions

Given that only limited areas in the world have both sufficiently high geothermal gradients and suitable reservoirs to allow for geothermal electricity production, it is important to focus on low-enthalpy geothermal heat applications.

This reviews shows that there is a large global geothermal resource base in sedimentary aquifers for direct heat use. With our method, we estimate a global geothermal resource base that ranges between 125 and 1793 EJ $yr^{-1}$. The mean heat flow through the total aquifer-overlain surface is 64 mW $m^{-2}$ and is similar to gross continental heat flow Our results show a mean aquifer geothermal gradient of 32 °C $km^{-1}$. Total effective aquifer volume ranges from $4.0{\cdot}10^{6}$ $km^{3}$ to $22.8{\cdot}10^{6}$ $km^{2}$.

Differences between the technical potential of greenhouse heating, spatial heating, and spatial cooling are explained by the spatial variation in aquifer thickness and geothermal gradients, combined with application-specific temperature requirements. From the three applications considered in this study, our results indicate that spatial cooling has the largest technical potential, followed by greenhouse heating and spatial heating. To obtain estimates for the economic potential and matched potential, global data on regional heat demand are needed.

There is an enormous potential for direct geothermal heat from aquifers: only 0.15% of the annual global final energy consumption is supplied by geothermal direct heat. The main causes for the large mismatch between potential and developed geothermal resources are high up-front costs for geothermal projects, decentralized production of geo-ther-mal heat, lack of uniformity among geothermal projects, geological uncertainties, and geotechnical risks. To increase the share of geothermal and other renewable heat sources, support policies are needed to remove financial and non-financial barriers.

## Acknowledgements

The research leading to these results has received funding from the European Community's Seventh Framework Programme under grant agreement no. 608553 (Project IMAGE). Part of the preliminary results have been shared in the Technology Roadmap for Geothermal Heat and

Power of the International Energy Agency (IEA) [33] and via the web-GIS viewer: http://www.thermogis.nl/worldviewer.

## References


[1] Cataldi R, Hodgson S, Lund J. (Eds.), Stories from a Heated Earth – Our Geothermal Heritage, Geothermal Resources Council and International Geothermal Association, Sacramento, California, USA, ISBN 0–934412–19–7, 1999.
[2] Fridleifsson I. Geothermal energy for the benefit of the people. Renew Sustain Energy Rev 2001;5:299–312.
[3] DiPippo R. Geothermal power plants: evolution and performance assessments. Geothermics 2015;53:291–307.
[4] Eisentraut A, Brown A. Heating without Global Warming: Market Developments and Policy Considerations for Renewable Heat, Tech. Rep., IEA (International Energy Agency), Paris, France, 2014.
[5] IPCC, Contribution of Working Groups I, II and III to the Fifth Assessment Report of the Intergovernmental Panel on Climate Change. In: Core Writing Team, R. Pachauri, L. Meyer (Eds.), Fifth Assessment Report of the Intergovernmental Panel on Climate Change, IPCC, Geneva, Switzerland, 151, 2015.
[6] Breede K, Dzebisashvili K, Liu X, Falcone G. A systematic review of enhanced (or engineered) geothermal systems: past, present and future, Geothermal Energy 1 (2013) 1–27.
[7] Olasolo P, Juárez M, D'Amico S, Liarte I. Enhanced geothermal systems (EGS): a review. Renew Sustain Energy Rev 2016;56:133–44.
[8] Lu S-M. A global review of enhanced geothermal system (EGS). Renew Sustain Energy Rev 2017:20. http://dx.doi.org/10.1016/j.rser.2017.06.097.
[9] Zang A, Oye V, Jousset P, Deichmann N, Gritto R, McGarr A, et al. Analysis of induced seismicity in geothermal reservoirs: an overview. Geothermics 2014;52:6–21.
[10] Heidbach O, Rajabi M, Reiter K, Ziegler M. World Stress Map 2016, GFZ Data Services, http://dx.doi.org/10.5880/WSM.2016.002, 2016.
[11] Gaucher E, Schoenball M, Heidbach O, Zang A, Fokker P, van Wees J-D, et al. Induced seismicity in geothermal reservoirs: a review of forecasting approaches. Renew Sustain Energy Rev 2015;52:1473–90.
[12] Kaya E, Zarrouk S, O'Sullivan M. Reinjection in geothermal fields – a review of worldwide experience. Renew Sustain Energy Rev 2011;15:47–68.
[13] Diaz AR, Kaya E, Zarrouk S. Reinjection in geothermal fields – a worldwide review update. Renew Sustain Energy Rev 2016;53:105–62.
[14] Gringarten A. Reservoir lifetime and heat recovery factor in geothermal aquifers used for urban heating. Pure Appl Geophys 1997;117:297–308.
[15] Willems C, Nick H, Donselaar M, Weltje G, Bruhn D. On the connectivity anisotropy in fluvial Hot Sedimentary Aquifers and its influence on geothermal doublet performance. Geothermics 2017;65:222–33.
[16] Willems C, Nick H, Goense T, Bruhn D. The impact of reduction of doublet well spacing on the net present value and the life time of fluvial hot sedimentary aquifer doublets. Geothermics 2017;68:54–66.
[17] Lopez S, Hamm V, Brun M Le, Schaper L, Boissier F, Cotiche C, et al. 40 years of Dogger aquifer management in Île-de-France. Paris Basin, Fr, Geotherm 2010;39:339–56.
[18] Axelsson G. Sustainable geothermal utilization - case histories; definitions; research issues and modelling. Geothermics 2010;39:283–91.
[19] Ungemach P, Antics M, Papachristou M. Sustainable Reservoir Management. In: Proceedings of the world geothermal congress 2005, The International Geothermal Association, Antalya, Turkey, 2005.
[20] Le Brun M, Hamm V, Lopez S, Ungemach P, Antics M, Ausseur J, Cordier E, Giuglaris E, Goblet P, Lalos P. Hydraulic and thermal impact modelling at the scale of the geothermal heating doublet in the Paris Basin. In: Proceedings of the Thirty-Sixth Workshop on Geothermal Reservoir Engineering 2011, Stanford University, Stanford, California, USA; 2011.
[21] Rybach L. Geothermal sustainability. GHC Bull 2007;28:2–7.
[22] Rybach L. Geothermal energy: sustainability and the environment. Geothermics 2003;32:463–70.
[23] Shortall R, Davidsdottir B, Axelsson G. Geothermal energy for sustainable development: a review of sustainability impacts and assessment frameworks. Renew Sustain Energy Rev 2015;44:391–406.
[24] Frick S, Kaltschmidt M, Schröder G. Life cycle assessment of geothermal binary power plants using enhanced low-temperature reservoirs. Energy 2010;35:2281–94.
[25] Bayer P, Rybach L, Blum P, Brauchler R. Review on life cycle environmental effects of geothermal power generation. Renew Sustain Energy Rev 2013;26:446–63.
[26] Menberg K, Pfister S, Blum P, Bayer P. A matter of meters: state of the art in the life cycle assessment of enhanced geothermal systems. Energy Environ Sci 2016;9:2720–43.
[27] Li K, Bian H, Liu C, Zhang D, Yang Y. Comparison of geothermal with solar and wind power generation systems. Renew Sustain Energy Rev 2015;42:1464–74.
[28] Lund J, Boyd T. Direct utilization of geothermal energy 2015 worldwide review. Geothermics 2016;60:66–93.
[29] REN21, Renewables 2017 Global Status Report, REN21 Secretariat, Paris, France, ISBN 978–3–9818107–6–9, 2017.
[30] van Sark W, Schepers J, van Wees J-D. The growing role of photovoltaic solar, wind and geothermal energy as renewables for electricity generation. Dewulf J, Meester SD, Alvarenga R, editors. Sustainability Assessment of Renewables-Based Products: Methods and Case Studies, 18. Ltd, Chichester, UK: John Wiley & Sons; 2015. [ISBN 9781118933916].
[31] Bertani R. Geothermal power generation in the world 2010–2014 update report. Geothermics 2016;60:31–43.
[32] Stefansson V. World Geothermal Assessment. In: Proceedings of the World Geothermal Congress 2005, The International Geothermal Association, Antalya, Turkey, 2005.
[33] International Energy Agency (IEA), Technology Roadmap: Geothermal Heat and Power, Organisation for Economic Co-Operation and Development, Tech. Rep., (OECD)/EIA, France, 2011.
[34] Fridleifsson I, Bertani R, Huenges E, Lund J, Ragnarsson A, Rybach L. The possible role and contribution of geothermal energy to the mitigation of climate change. In: O. Hohmeyer, T. Trittin, (Eds.), IPCC Scoping Meeting on Renewable Energy Sources - Proceedings, Lübeck, Germany, 2008, 59–80.
[35] Goldstein B, Hiriart G, Bertani R, Bromley C, Gutiérrez-Negrín L, Huenges E, et al. IPCC special report on renewable energy sources and climate change mitigation. In: Edenhofer O, Pichs-Madruga R, Sokona Y, Seyboth K, Matschoss P, Kadner S, Zwickel T, Hansen PEG, Schlömer S, von Stechow C, editors. Geothermal Energy. Cambridge, United Kingdom and New York, NY, USA: Cambridge University Press; 2011. p. 401–36. [ISBN 978-1-107-02340-6].
[36] van Wees J-D, Kronimus A, van Putten M, Pluymaekers M, Mijnlieff H, van Hooff P, et al. Geothermal aquifer performance assessment for direct heat production - methodology and application to Rotliegend aquifers. Geol Mijnbouw J G 2012;91:651–65.
[37] Beckers K, Lukawski M, Anderson B, Moore M, Tester J. Levelized costs of electricity and direct-use heat from Enhanced Geothermal Systems. J Renew Sustain Energy 2014;6:013141.
[38] Gehringer M, Loksha V. Geothermal Handbook: Planning and Financing Power Generation, ESMAP (Energy Sector management Assistance Programme) Technical report no. 002/12, Tech. Rep., The International Bank for Reconstruction And Development / The World Bank Group, Washington, DC, USA, 2012.
[39] Netherlands Enterprise Agency (RVO.nl) commissioned by the ministery of Economic Affairs, Risico's dekken voor Aardwarmte: Garantieregeling tegen het risico van misboring [Risks Cover for Thermal Energy: Guarantee scheme against the risk of unsuccessful drilling], Tech. Rep., Netherlands Enterprise Agency (RVO.nl), Roermond, The Netherlands, 2016.
[40] Thorsteinsson H, Tester J. Barriers and enablers to geothermal district heating system development in the United States. Energy Policy 2010;38:803–13.
[41] Sanchez-Alfaro P, Sielfeld G, Van Campen B, Dobson P, Fuentes V, Reed A, et al. Geothermal barriers, policies and economics in Chile Lessons for the Andes. Renew Sustain Energy Rev 2015;51:1390–401.
[42] Muffler P, Caltaldi R. Methods for regional assessment of geothermal resources. Geothermics 1978;7:53–89.
[43] Williams C. Updated methods for estimating recovery factors for geothermal resources. In: Proceedings of the thirty-second workshop on geothermal reservoir engineering 2007, Stanford University, Stanford, California, USA; 2007.
[44] Blackwell D, Negraru P, Richards M. Assessment of the enhanced geothermal system resource base of the United States. Nat Resour Res 2007;15:283–308.
[45] Kramers L, van Wees J-D, Pluymaekers M, Kronimus A, Boxem T. Direct heat resource assessment and subsurface information systems for geothermal aquifers; the Dutch perspective. Geol Mijnbouw-N J G 2012;91:637–49.
[46] Limberger J, Calcagno P, Manzella A, Trumpy E, Boxem T, Pluymaekers M, et al. Assessing the prospective resource base for enhanced geothermal systems in Europe. Geotherm Energy Sci 2014;2:55–71.
[47] Beardsmore G, Rybach L, Blackwell D, Baron C. Protocol for estimating and mapping the global EGS potential. Geotherm Res T 2010;34:301–12.
[48] Grant M. Stored-heat assessments: a review in the light of field experience. Geotherm Energy Sci 2014;2:49–54.
[49] Daniilidis A, Alpsoy B, Herber R. Impact of technical and economic uncertainties on the economic performance of a deep geothermal heat system. Renew Energy 2017;114B:805–16.
[50] Gargs S, Combs J. A reformulation of USGS volumetric heat in place resource estimation method. Geothermics 2015;55:150–8.
[51] Athy L. Density, porosity and compaction of sedimentary. AAPG Bull 1930;14:1–24.
[52] Hantschel T, Kauerauf A. Fundamentals of basin and petroleum systems modeling. Berlin, Heidelberg, Germany: Springer; 2009. [ISBN 978-3540723172].
[53] Tesauro M, Kaban M, Cloetingh S. EuCRUST-07: a new reference model for the European crust. Geophys Res Lett 2008;35:1–5.
[54] Laske G, Masters G. A Global Digital Map of Sediment Thickness, EOS Transactions AGU 78, F483.
[55] Exxon Production Research Company, Tectonic map of the world, Tech. Rep., American Association of Petroleum Geologists (AAPG) Foundation, Tulsa, Oklahoma, USA, 1985.
[56] Lukawski M, Anderson B, Augustine C, Capuano L, Beckers K, Livesay B, et al. Cost analysis of oil, gas, and geothermal well drilling. J Petrol Sci Eng 2014;118:1–14.
[57] Cloetingh S, van Wees J-D, Ziegler P, Lenkey L, Beekman F, Tesauro M, et al. Lithosphere tectonics and thermo-mechanical properties: an integrated modelling approach for Enhanced Geothermal Systems exploration in Europe. Earth-Sci Rev 2010;102:159–206.
[58] Moeck I. Catalog of geothermal play types based on geologic controls. Renew Sustain Energy Rev 2014;37:867–82.
[59] Pluymaekers M, Kramers L, van Wees J-D, Kronimus A, Boxem SNT, Bonté D. Reservoir characterisation of aquifers for direct heat production: methodology and screening of the potential reservoirs for the Netherlands. Geol Mijnbouw-N J G 2012;91:621–36.
[60] Lund J. Direct utilization of geothermal energy. Energies 2010;3:1443–71.
[61] Luijendijk E, ter Voorde M, van Balen R, Verweij H, Simmelink E. Thermal state of the Roer Valley Graben, part of the European Cenozoic Rift System. Basin Res

2011;23:65–82.
[62] Kooi H. Groundwater flow as a cooling agent of the continental lithosphere. Nat Geosci 2016;9:227–30.
[63] Bierkens M. Global hydrology 2015: state, trends, and directions. Water Resour Res 2015;51:4923–47.
[64] Limberger J, Bonté D, de Vicente G, Beekman F, Cloetingh S, van Wees J-D. A public domain model for 1D temperature and rheology construction in basement-sedimentary geothermal exploration: an application to the Spanish Central System and adjacent basins. Acta Geod Geophys 2017;52:269–82.
[65] Fuchs S, Schütz F, Förster H-J, Förster A. Evaluation of common mixing models for calculating bulk thermal conductivity of sedimentary rocks: correction charts and new conversion equations. Geothermics 2013;47:40–52.
[66] Artemieva I. Global $1^{\circ}$x$1^{\circ}$ thermal model TC1 for continental lithosphere: implications for lithosphere secular evolution. Lithos 2006;109:23–46.
[67] Pollack H, Hurter S, Johnson J. Heat flow from the Earth's interior: analysis of the global data set. Rev Geophys 1993;31:267–80.
[68] Davies J. Global map of solid Earth surface heat flow. Geochem Geophys Geosyst 2013;14:4608–22.
[69] Blackwell D, Richards M, Frone Z, Batir J, Williams M, Ruzo A, Dingwall R. SMU Geothermal Laboratory Heat Flow Map of the Conterminous United States, 2011, SMU Geothermal Laboratory, ⟨http://smu.edu/geothermal⟩, 2011.
[70] Global Volcanism Program, Volcanoes of the World, v. 4.5.0. Venzke E (ed.), Smithsonian Institution, http://dx.doi.org/10.5479/si.GVP.VOTW4-2013 Downloaded 01 Jul 2016, 2013.
[71] Nagao T, Uyeda S. Methods for regional assessment of geothermal resources. Tectonophysics 1995;251:153–9.
[72] Hijmans R, Cameron S, Parra J, Jones P, Jarvis A. Very high resolution interpolated climate surfaces for global land areas. Int J Climatol 2005;25:1965–78.
[73] Kalnay E, Kanamitsu M, Kistler R, Collins W, Deaven D, Gandin L, et al. He NCEP/NCAR 40-year reanalysis project. Bull Am Meteorol Soc 1996;77:437–70.
[74] Boyer T, Antonov J, Baranova O, Coleman C, Garcia H, Grodsky A, Johnson D, Locarnini R, Mishonov A, O'Brien T, Paver C, Reagan J, Seidov D, Smolyar I, Zweng M. World Ocean Database 2013. in: S. Levitus, A. Mishonov (Eds.), NOAA Atlas NESDIS 72, NOAA, Silver Spring, Maryland, USA, 209, 2013.
[75] Amante C, Eakins B. ETOPO1 1 Arc-Minute Global Relief Model: Procedures, Data Sources and Analysis, NOAA Technical Memorandum NESDIS NGDC-24, ⟨http://www.ngdc.noaa.gov/mgg/global/relief/ETOPO1/docs/ETOPO1.pdf⟩, 2009.
[76] Barbier E, Fanelli M. Non-electrical uses of geothermal energy. Prog Energy Combust 2012;91:637–49.
[77] Barbier E. Nature and technology of geothermal energy: a review. Renew Sustain Energy Rev 1997;1:1–2.
[78] Barbier E. Geothermal energy technology and current status: an overview. Renew Sustain Energy Rev 2002;6:3–65.
[79] Rubio-Maya C, Díaz VA, Martínez EP, Belman-Flores J. Cascade utilization of low and medium enthalpy geothermal resources – a review. Renew Sust Energ Rev 2015;52:689–716.
[80] Rybach L. Classification of geothermal resources by potential. Geotherm Energy Sci 2015;3:13–7.
[81] Möller B, Nielsen S. High resolution heat atlases for demand and supply mapping, IJSEPM 1, 41–58.
[82] McCabe K, Gleason M, Reber T, Young K, Characterizing. U.S. heat demand for potential application of geothermal direct use. Geotherm Res T 2016;40:1032388.
[83] Heat Roadmap Europe, Pan-European Thermal Atlas 4.1, Europa-Universität, Halmstad University and Aalborg University, ⟨http://www.heatroadmap.eu/Peta4.php⟩[accessed 1 June 2017], 2017.
[84] Connoly D. Heat Roadmap Europe: Quantitative comparison between the electricity, heating, and cooling sectors for different European countries, Energy (2017) 38, http://dx.doi.org/10.1016/j.energy.2017.07.037.
[85] Jaupart C, Labrosse S, Mareschal J-C. Temperatures, heat and energy in the mantle of the in: D. Berdovici Earth, Schubert G. (Eds.) Treatise on Geophysics, vol. 7, chap. Mantle Convection, Elsevier, Amsterdam, The Netherlands, ISBN 978–0–444–52748–6, 2007, 253–303.
[86] EPRI, Geothermal energy prospects for the next 50 years, Tech. Rep. ER 611-SR, Electric Power Research Institute, Palo Alto, California, USA, 1978.
[87] Powell W, Chapman D, Balling N, Beck A. Continental heat-flow density. In: Haenel R, Rybach L, Stegena L, editors. Handbook of Terrestrial Heat-Flow Density Determination. Dordrecht, The Netherlands: Kluwer Academic Publishers; 1988. p. 167–222.
[88] Beardsmore G, Cull J. Crustal heat flow: a guide to measurement and modelling. Cambridge, UK: Cambridge University Press; 2001. [ISBN 0-521-79289-4].